3D Representation of UAV-obstacle Collision Risk Under Off-nominal conditions

Portia Banerjee
KBR, NASA Ames Research Center
Moffett Field, CA 94035
portia.banerjee@nasa.gov

George Gorospe
KBR, NASA Ames Research Center
Moffett Field, CA 94035
george.gorospe@nasa.gov

Ersin Ancel
NASA Langley Research Center,
1 NASA Dr, Hampton, VA 23666
ersin.ancel@nasa.gov

***Abstract*—Safe operations of autonomous unmanned aerial vehicles (UAVs) in low-altitude airspace with beyond visual line-of-sight (BVLOS) flights demand robust risk monitoring of airspace as well as of people and property on ground. One of the safety critical factors for UAV flights is the risk of collision with static and dynamic obstacles in proximity to its flight path. This paper presents a detailed formulation of risk likelihood of obstacle collision incorporating the effects of off-nominal conditions introduced by component failures, degraded controllability and environmental disturbances such as wind gusts. The deviation in the planned trajectory caused due to wind is computed utilizing a point-mass 3D kinematic simulation model of the vehicle. Likelihood of risk for the flight plan is then analyzed based on generating the probability of collision for each point in the trajectory. The proposed risk factor is demonstrated on real flight data from experimental flights of an octocopter at NASA Langley Research Center in presence of simulated obstacles and wind conditions. Effect of varying wind conditions, distance from obstacles, level of controllability and obstacle measurement noise on the risk factor is demonstrated. The proposed approach enables risk-informed decision making for timely mitigation of current and future unsafe events in autonomous systems.**

TABLE OF CONTENTS

1. INTRODUCTION

Emergence of unmanned aerial vehicles (UAVs) as a viable vehicle for commercial operations in urban airspace comes with crucial technical and safety challenges. With a variety of vehicles potentially operating in this space in addition to variations in weather, system health degradation and evolving operational concepts, there is a clear need for robust and system-wide risk monitoring of the airspace. At the vehicle level, risk assessment for routine operations beyond visual line of sight within these complex and evolving environments will identify relevant factors leading to potentially hazardous conditions and therefore aid in mitigation of such situations of high consequence.

As UAVs are considered for operations outside of research facilities, new and clear risks must be evaluated for safety and mission assurance. Safety monitoring frameworks similar to the ones developed for manned aircraft [1], [2] may enhance unmanned traffic management with in-time monitoring and prediction tools for low-altitude operating vehicles. NASA's Aeronautics Research Mission Directorate (ARMD) strategic plan directs the development of advanced in-time safety assurance tools that can monitor, assess and mitigate risks for UAV operations [3]. Under that initiative, several studies have been directed to prediction of future trajectory [4], [5], estimation of remaining battery life [6], estimation of vibrational anomalies [7] as well as assessment of risk to population on ground in the event of a crash [8]. A vital step towards safety assessment of the unmanned airspace is the formulation and development of methods for UAV-obstacle collision risk during off-nominal conditions. While static obstacles, such as buildings, trees, utility poles etc., may be mapped and thus easier to avoid, a variety of factors including weather conditions, the presence of wind and/or gusts or reduced control capability can create a higher risk of collision with these objects.

Clothier and Walker provide a concise exploration of the challenges associated with the application of risk assessment and management towards the achieving and "acceptable level" of risk in UAV operations [9]. Weibel, Roland, and Hansman performed a preliminary hazard analysis for both ground impact and midair collisions using risk models for a range of UAV classifications and capabilities, and found that risk varied significantly based on population density, the mass of the vehicle, and the cruise speed [10]. Weinert et. al. used a monte-carlo driven risk assessment of UAV operations to evaluate the safety of small UAV well-clear definitions, determining that for small UAVs a smaller well-clear definition compared with TCAS alerting criteria is tolerable [11]. Primatesta, Guglieri, and Rizzo approached the risk assessment for a given trajectory with a risk-map wherein each cell the 2D space has a risk-cost as defined by the subsequent three probabilities, loss of control and ground impact, impact with a person, and fatal injury to an impacted person [12]. Belkhouche also derives a model for UAV collision risk assessment accounting for uncertainties utilizing a Monte Carlo method [13]. Lee, Meyn, and Kim, utilized actual traffic data collected over a one-year period for their traffic model and probabilistic approach to safety assessment [14]. Hu similarly created a probabilistic risk-based approach to defining a safety bound, using both a Monte Carlo simulation for uncertainty quantification, and a reinforcement learning algorithm for collision avoidance and trajectory planning [15].

While literature features other examples of risk assessment for UAVs, this paper details the formulation of risk likelihood caused by deviation in its planned trajectory towards an obstacle. The risk matrix framework is described in section 2 followed by definition for probability of collision in terms of wind speed, direction, controllability and obstacle

measurement noise. Finally, the risk assessment framework is applied to a real UAV flight data for a region augmented with simulated obstacles.

2. Risk of Obstacle Collision Framework

In a previous study, Ancel et al. defined the non-participant casualty risk in terms of expected casualties on the ground in the event of an unpowered descent of an UAV under off-nominal conditions [16]. The authors employed a modified version of the risk matrix highlighted within the FAA's Safety Management System Manual [17] to establish and visualize real time UAS flight risks. As part of the obstacle collision risk estimation, a similar risk matrix (Fig.1) was used to represent and track associated risks. The rows in the matrix represent likelihood of UAS collision with buildings based on off-nominal condition such as presence of wind, vehicle controllability, vehicle size, and obstacle noise whereas the columns provide severity categories which is considered to be probability of causing one or more casualties on the ground or within buildings. The final risk associated with an event is computed as the product of its likelihood and severity and categorized as low (green), medium (yellow) and high (red) risk events. However, at the time of writing, the FAA does not provide specific guidance on likelihood and severity definitions for unmanned aircraft flight operation risk over populated areas, thus, the acceptable thresholds for severity (minimal, minor, major, catastrophic) and likelihood (frequent, probable, remote, and improbable) were chosen arbitrarily here for the purposes of concept evaluation and demonstration [8].

Severity → Likelihood↓	Minimal $0 < P_{casualty} \leq 0.25$	Minor $0.25 < P_{casualty} \leq 0.5$	Major $0.5 < P_{casualty} \leq 0.75$	Catastrophic $0.75 < P_{casualty} \leq 1$
Frequent $0 < P_{coll-obs} \leq 0.25$				
Probable $0.25 < P_{coll-obs} \leq 0.5$				
Remote $0.5 < P_{coll-obs} \leq 0.75$				
Improbable $0.75 < P_{coll-obs} \leq 1$				

Figure 1: Notional risk matrix adopted from [16].

$$Risk_{obs} = P_{coll-obs} \times P_{casualty} \tag{1}$$

The UAV's risk of collision with obstacles under off-nominal conditions was given in Eq. (1), expressed by the product of likelihood of such a collision and the expected severity of the outcomes. For unmanned operations, the severity can be defined as the casualty risk to non-participants in the event of a collision with buildings or the ground [8]. Using Eq. (2), the casualty area expression can be modified to include controlled decent into terrain (due to a vertical trajectory deviation) where the impact angle, γ, can be obtained from the aircraft trajectory within the aircraft system parameters.

$$A_c = \pi(R_p + R_{uav})^2 + 2(R_p + R_{uav})\frac{H_p}{\tan\gamma} \tag{2}$$

For the cases where the aircraft collides with a building face, the impact angle would depend on the approach angle with respect to the building, however, the aircraft can be assumed to follow a straight trajectory to the ground where $\gamma = 90°$. Alternatively, based on the aircraft kinetic energy and building roof/facade material, it is possible to estimate casualty values within the buildings by the use of penetration models as described in [16]. Finally, by modifying the A_c expression, the probability of having n or more casualties in a populated area can be computed, as defined in [8].

The other component of risk is the risk likelihood which is proposed in this paper as a function of probability of trajectory deviation caused by wind $p_{traj-dev}$, area of the vehicle exposed to the obstacle when subjected to collision A_{exp} and probability that the point of collision represents an obstacle p_{obst}.

$$P_{coll-obs} = p_{traj-dev}\ A_{exp}\ p_{obst} \tag{3}$$

The primary critical parameter in the risk likelihood formulation is the probability of trajectory deviation $p_{traj-dev}$ which depends on a number of factors such as proximity of UAV from the obstacle, local wind field magnitude and direction as well as the state-of-health of the propeller unit. Effects of each of these factors on the risk likelihood is formulated in section 3 and results are demonstrated in section 4 of this paper.

3. Factors Affecting Probability of Collision with Obstacle

Effect of wind

A 3-dimensional kinematic point-mass model is used to incorporate the effect of wind on trajectory deviation by the UAV [18], [19]. The vehicle state is described by the UAV airspeed V, heading (χ) determined by the directional path from one waypoint to another and flight path angle (γ). The 3D coordinates of each waypoint is defined by its longitude (θ), latitude (ϕ), and altitude (h). The vehicle velocity $\vec{V_{UAV}}$ given heading (χ) and flight path angle (γ) is given by Eq. (4), where $\hat{i}, \hat{j}$ and $\hat{k}$ represents the unit vectors in the ground reference frame.

$$\vec{V_{UAV}} = V\cos\gamma\cos\chi\hat{i} + V\cos\gamma\sin\chi\hat{j} + V\sin\gamma\hat{k} \tag{4}$$

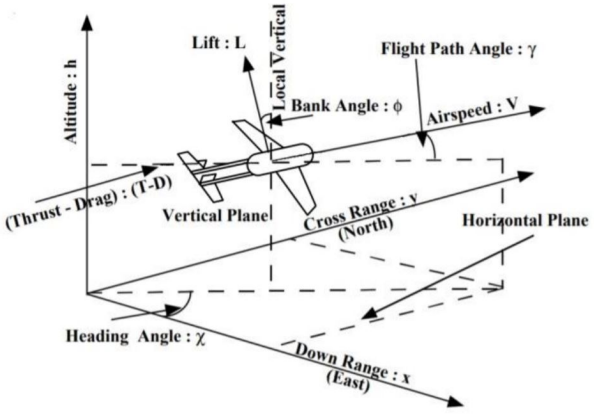

Figure 2: UAV coordinate system [18].

Considering wind velocity vector as $\vec{V}_{wind}$ and obtaining vehicle's cruise speed $\vec{V_{UAV}}$ from Eq. (4), the total vehicle

velocity is given by $\vec{V}_{total}$.

$$\vec{V}_{wind} = U\hat{i} + V\hat{j} + W\hat{j} \tag{5}$$

$$\vec{V}_{total} = \vec{V_{UAV}} + \vec{V}_{wind} \tag{6}$$

The flight path angle (γ) is defined in the angle between the direction at which the vehicle's nose is pointing and the course over ground, as shown in Figure 2. If $\gamma = 0$ under no-wind condition, any non-zero value of γ during a UAV flight is caused by the vertical component of the instantaneous wind speed. Therefore the induced flight angle γ_{wind} after deviated vertically by wind is described by equation (7).

$$\gamma_{wind} = \arctan \frac{W}{V\cos\gamma + U} \tag{7}$$

Similarly, the horizontal deviation of the vehicle changes its heading (χ) and is caused by the horizontal components of the wind. Given the estimated time from detection of disturbance on the vehicle to its recovery to original trajectory is denoted by $t_{control}$, the new position of the UAV deviated by wind $(\theta_{dev}, \phi_{dev}, h_{dev})$ at every position in the original reference trajectory $(\theta_{ref}, \phi_{ref}, h_{ref})$ is given by Eqs. (8)-(10).

$$\theta_{dev} = t_{control}\frac{|\vec{V}_{total}|\sin\chi}{R\cos\phi_{ref}} + \theta_{ref} \tag{8}$$

$$\phi_{dev} = t_{control}\frac{|\vec{V}_{total}|\cos\chi}{R} + \phi_{ref} \tag{9}$$

$$h_{dev} = t_{control}\,|\vec{V}_{total}|\,\sin\gamma_{wind} + h_{ref} \tag{10}$$

Collision with an obstacle occurs when the deviated position of the UAV $(\theta_{dev}, \phi_{dev}, h_{dev})$ hits or lies within the boundary of an obstacle. In practical applications, the wind velocity is measured or estimated at every point on the trajectory and be associated with stochasticity depending on the sensor characteristics and estimation process. Assuming Gaussian distribution of the wind field velocity is interpreted in terms of n_s samples associated with probabilities, each deviated position in the trajectory is computed for n_s samples, according to Eqs. (8)-(10). The samples which are deviated and hit or lie within the boundary of any obstacle after $t_{control}$ seconds are identified as the collided samples n_{dev} and the probability of obstacle collision $p_{traj-dev}$ is defined in Eq. (3).

$$p_{traj-dev} = \frac{n_{dev}}{n_s} \tag{11}$$

Effect of controllability

As denoted in Eqs. (8)-(10), the shift in the position of the UAV during its flight is dependent on the control time $t_{control}$ which in turn is dependent on the UAV controller characteristics, vehicle type and state-of-health of its maneuver components. In case of a healthy rotorcraft vehicle, the control time can be assumed to be 1 sec. If a motor degradation is identified, the maneuverability of the UAV is affected which increases the time taken by the vehicle to recover from a sudden deviation. Hence value to $t_{control} \geq 1$ results in higher risk of obstacle collision.

Effect of obstacle noise

In Eq. (3), p_{obst} is computed based on the error associated with obstacle measurements. For fixed obstacles such as trees and buildings, the obstacle locations and sizes are typically obtained from navigation sensors such as GNSS, IMU, LiDAR and cameras [20] which may be associated with intrinsic measurement noise. If the error or noise in the navigation measurements is assumed to adhere to a normal distribution with mean μ and variance of σ^2, the p_{obst} can be defined as the cumulative distribution function, denoted in Eq. (12) which then feeds into Eq. (3) for computation of the probability of collision. Here x is the position at which collision with the obstacle takes place, as shown in figure 3.

$$p_{obst} = \frac{1}{2}[1 + \mathrm{erf}(\frac{x-\mu}{\sigma_{obs}\sqrt{2}})] \tag{12}$$

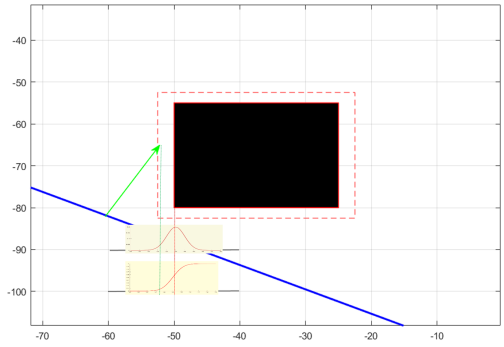

Figure 3: Schematic of p_{obst} calculation.

4. RISK ASSESSMENT RESULTS

The probability of obstacle collision is computed for an experimental UAV flight conducted at the NASA Langley Research Center. Figure 4 (b) shows the flight plan executed with a *DJI S1000* Octocopter in autonomous mode. The vehicle, as depicted in figure 4 (a), was equipped with Pixhawk autopilot hardware (*http://pixhawk.org/*) and commanded with Ardupilot software (*http://ardupilot.org/*) to fly through pre-defined 9 waypoints in almost 7 minutes.

Figure 4b shows the vehicle location "unrolled in time", calculated by the autopilot using GPS locations and its inertial measurement unit. The geospatial coordinates (latitude, longitude, and altitude) have been converted into a local, Earth-fixed reference frame with origin at the take-off location, x-axis pointing East, y-axis pointing North, and z-axis pointing upwards, forming a East-North-Up (ENU) reference frame. The z-axis represents altitude of the flight relative to its starting location which was from the top of a building. The UAV landed on the ground at certain times during the flight which are hence represented by the negative z-values.

For implementing the proposed risk assessment approach, the above flight data was used in a playback mode with simulated obstacles denoted by the red boxes in figure 5a where the arrows state the vehicle direction. At first,the flight trajectory is generated from the waypoint locations and commanded ETAs, using a modified B-spline algorithm presented in an earlier study [4]. The corresponding planned velocity profile of the UAV is computed under no-wind conditions, as represented in figure 5b.

A simulated wind profile is added to the above trajectory.

(a)

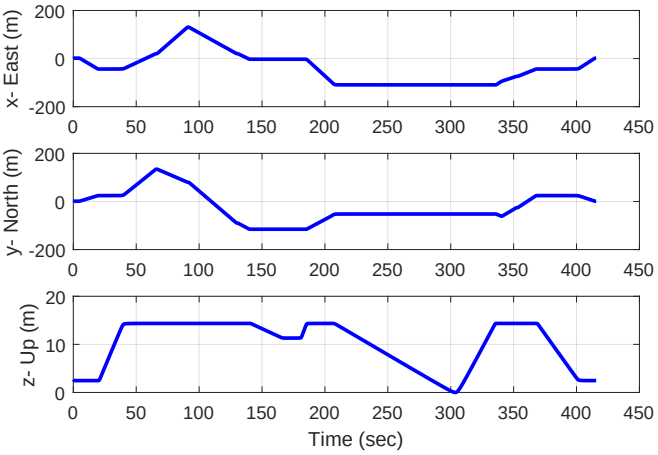

(b)

Figure 4: Example of DJIS1000 octocopter (4a) test flight in autonomous mode: the observed position is compared against the flight plan in a East-North-Up reference frame (4b).

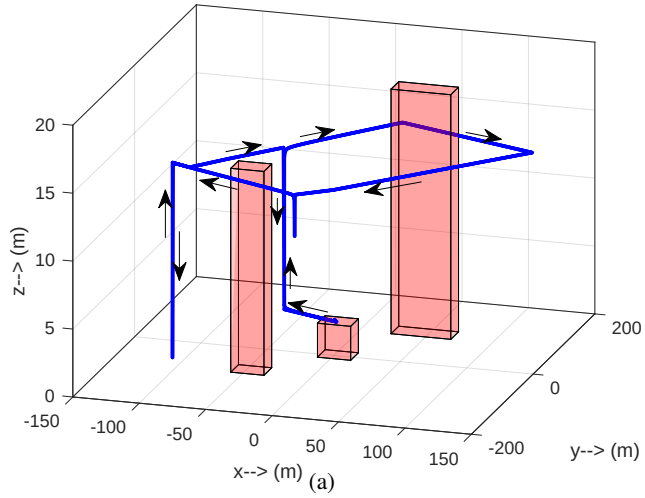

(a)

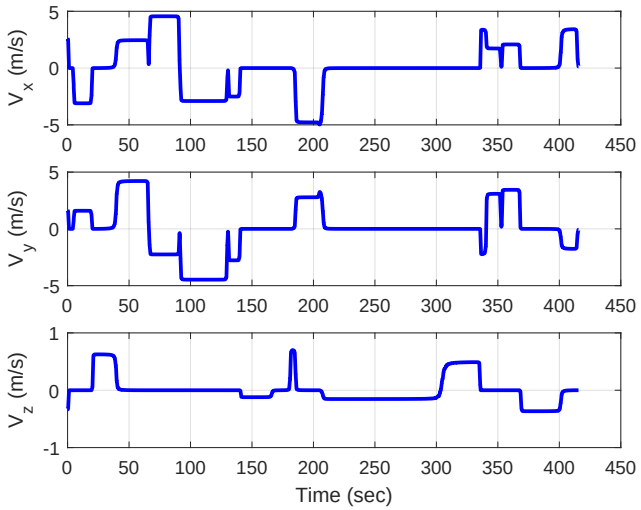

(b)

Figure 5: (a) Flight plan in 3D with simulated obstacles as red boxes (b) Velocity profile of the planned flight under no-wind condition.

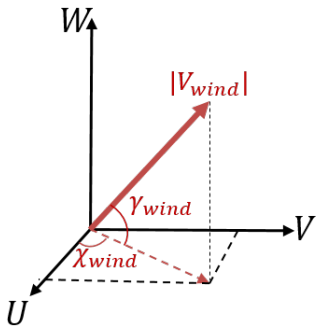

Figure 6: Wind coordinates in 3D representation.

Probability of the obstacle collision is computed under different wind conditions by varying wind speed magnitude $|V_{wind}|$ and direction. Direction of the wind field is defined in terms of two angles as shown in figure 6: (i) γ_{wind}: angle between wind velocity vector and the x-y plane and (ii) χ_{wind}: angle between wind velocity vector and the x-plane. Fixing the wind speed parameters at $|V_{wind}| = \mathcal{N}(10, 2)\, ms^{-1}$, $\chi_{wind} = -120°$ and $\gamma_{wind} = 2°$, the corresponding normalized risk of obstacle collision is plotted in figure 7. Depending on the intensity and direction of the wind acting at each point on the trajectory and the surrounding obstacle location, the deviated positions may or may not lead to a collision and hence the probability of collision varies accordingly. The risk likelihood is normalized such that the final value lies between 0 and 1. As shown in the legend, risk is zero for most of the trajectory. It is only a smaller section of the flight plan that lies in close proximity to one of the obstacles where the risk increases to approximately 0.7. It should be noted that although another section of the trajectory lies close to the other obstacle, the risk is zero in that section on account of the wind direction. In the presence of a stationary wind field, the probability of collision with an obstacle is not only dependent on the distance of the obstacle from the flight plan, but also on the wind direction that decides if the deviated position of the vehicle hits an obstacle or not.

The effect of wind on risk likelihood is evaluated in figure 8 where the UAV with the assumption of healthy maneuverability conditions is subjected to three different winds of magnitude of $2ms^{-1}, 5ms^{-1}$ and $8ms^{-1}$. The wind direction is fixed at $\chi_{wind} = -120°$ and $\gamma_{wind} = -5°$. As observed, risk of obstacle collision increases with wind magnitude, as expected.

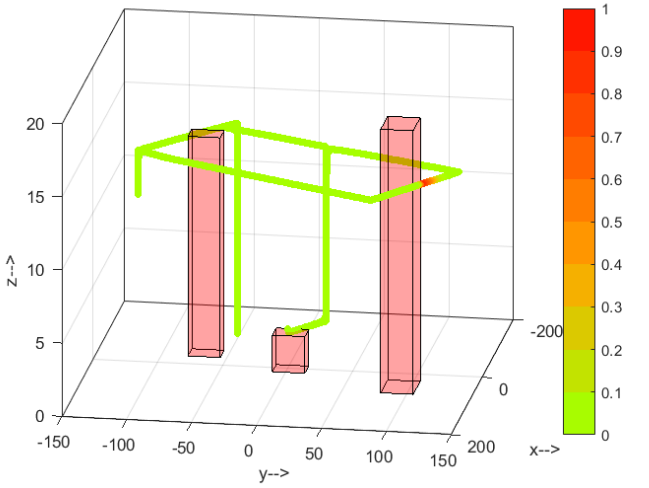

Figure 7: Probability of obstacle collision in presence of wind with $|V_{wind}| = \mathcal{N}(8,2)m/s$, $\chi_{wind} = -120°$ and $\gamma_{wind} = 2°$.

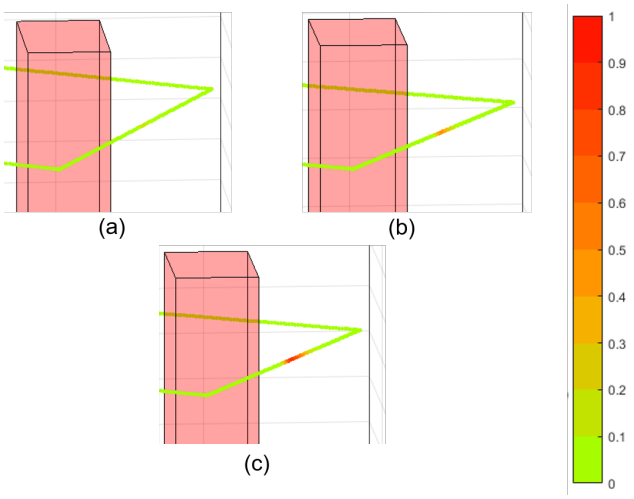

Figure 8: Effect of wind on Probability of obstacle collision. Wind 1: $|V_{wind}| = \mathcal{N}(2,2)m/s$, ; Wind 2: $|V_{wind}| = \mathcal{N}(5,2)m/s$; Wind 3: $|V_{wind}| = \mathcal{N}(8,2)m/s$.

Finally, effect of distance from the obstacle, wind speed and wind direction on the risk of obstacle collision are shown in figure 9. Figure 9 (a) denotes that for a fixed wind magnitude of $|V_{wind}| = \mathcal{N}(5,2)m/s$ and direction $\chi_{wind} = 70°$ and $\gamma_{wind} = -5°$, the risk of obstacle collision risk reduces with increase in the distance from the obstacle. This plot enables to identify the minimum 'safe' distance of the trajectory from obstacle at $7.3m$ that is associated with a risk of 0.1. Hence by fixing the flight trajectory at a safe distance of $7.3m$ away from the obstacle, the risk was calculated for increasing magnitude of wind as shown in figure 9 (b). As observed, the risk increases with increasing wind magnitude and a risk of 0.1 is achieved at $|V_{wind}| = \mathcal{N}(4.8,2)m/s$. Finally, risk was calculated for varying wind direction χ from $5°$ to $120°$ in order to demonstrate its its effect on safety. In this section of the flight trajectory, the UAV flew at $\chi = 150°$, hence $\chi = 60°$ represents a cross-wind which causes highest probability of trajectory deviation and hence maximum risk likelihood. Such parametric studies aids in computing the

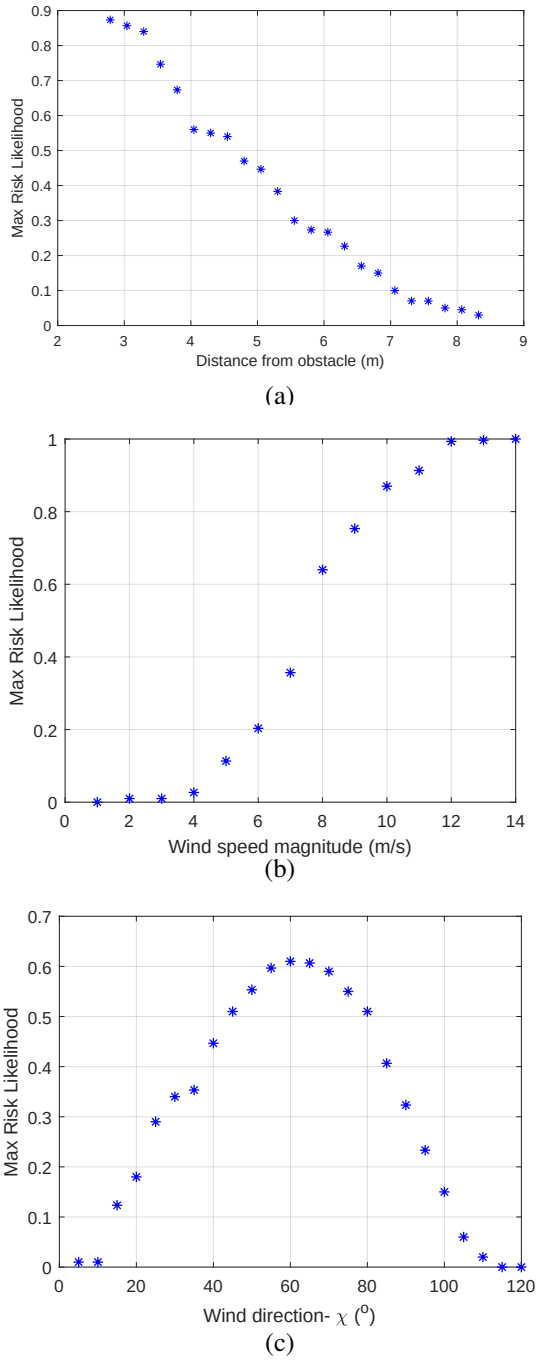

Figure 9: (a) $P_{coll-obs}$ with varying distance from obstacle at $|V_{wind}| = \mathcal{N}(5,2)m/s$,$\chi_{wind} = 70°$ and $\gamma_{wind} = -5°$. (b)$P_{coll-obs}$ with varying wind speed at $\chi_{wind} = 70°$, $\gamma_{wind} = -5°$ and $7.3m$ away from obstacle (c) $P_{coll-obs}$ with varying wind direction χ_{wind} at $|V_{wind}| = \mathcal{N}(8,2)m/s$, $\gamma_{wind} = -5°$ and $7.3m$ away from obstacle.

safe thresholds while planning a flight as well as resolving in-time contingencies when exposed to off-nominal conditions during a flight.

Another important factor that affects collision risk for a UAV is its controllability or maneuverability conditions. If the controllability is compromised due to a degraded motor or

any other propeller unit, the control time increases which is then reflected in the increased risk likelihood. Figure 10 denotes two risk plots for the same UAV subjected to the same simulated wind but at different control times: (a) $t_{control} = 1sec$ and (b) $t_{control} = 2sec$. The UAV with degraded controllability experiences higher risk likelihood in its planned trajectory as well as for a greater section of the trajectory, as denoted in figure 10 (b).

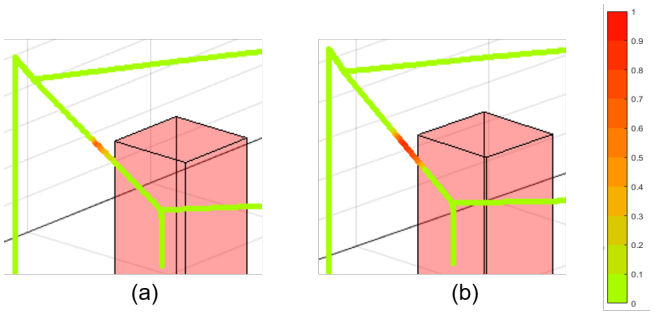

Figure 10: Effect of controllability on Probability of obstacle collision with wind at $|V_{wind}| = \mathcal{N}(5,2)m/s$, $\chi_{wind} = 60°$ and $\gamma_{wind} = -5°$ (a) $t_{control} = 1sec$ and (b) $t_{control} = 2sec$.

Finally, effect of obstacle measurement noise is shown in Figure 11 where the risk likelihood is plotted for two cases of noise variance associated with the obstacle measurements (a) $\sigma_{obs} = 0.05$ and (b) $\sigma_{obs} = 1.5$. The distance of the obstacle from the trajectory as well as wind conditions and vehicle controllability are kept constant for the two cases at $dis = 7.3m$, $|V_{wind}| = \mathcal{N}(7,2)m/s$, $\chi_{wind} = 60°$ and $\gamma_{wind} = -5°$. The probability that the collision point represents an obstacle is computed according to equation (12) which then feeds into Eq.(3). It is observed that increase of measurement noise increases likelihood for the same section of the trajectory.

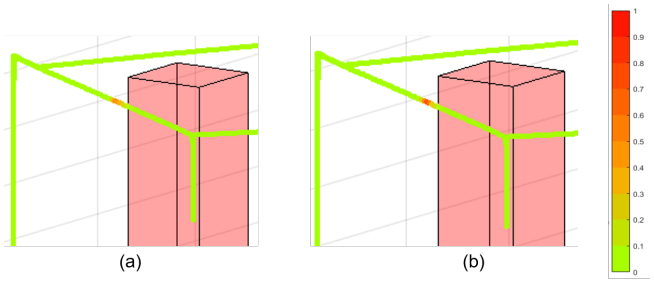

Figure 11: Effect of obstacle measurement noise on Probability of obstacle collision (a) $max(P_{coll-obs}) = 0.3$ with $\sigma_{obs} = 0.05$ and (b) $max(P_{coll-obs}) = 1.5$ with $\sigma_{obs} = 1.2$.

The relationship between obstacle measurement noise and risk likelihood is further depicted in Figure 12. It should be noted that even when σ_{obs} is close to zero, the risk likelihood is 0.48 since the wind magnitude ($(7,2)m/s$) is high enough to generate a high probability of collision even without obstacle measurement noise.

5. Conclusion

In this paper, the risk of obstacle collision has been defined for an autonomous UAV. The probability of collision with an obstacle is formulated as a function of multiple parameters

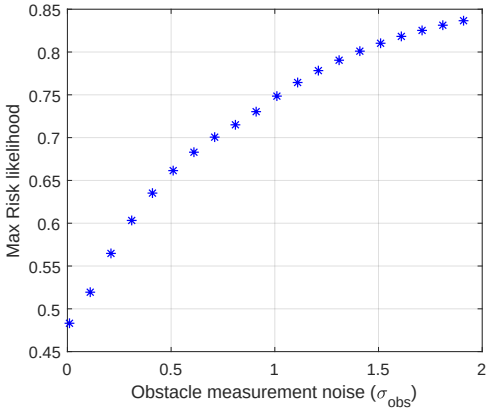

Figure 12: $P_{coll-obs}$ with varying obstacle measurement noise (σ_{obs}) at $|V_{wind}| = \mathcal{N}(5,2)m/s$,$\chi_{wind} = 70°$, $\gamma_{wind} = -5°$ and $7.3m$ away from obstacle.

including the probability of trajectory deviation towards obstacles, the area of exposure and obstacle measurement noise. The effect of wind speed magnitude, direction and vehicle controllability is incorporated in the definition of probability of trajectory deviation towards obstacles. Moreover, effect of these individual parameters on the overall risk likelihood is demonstrated on a real UAV flight augmented in a simulated environment. Further, safety requirements in terms of minimum distance from obstacle and maximum wind tolerance are obtained from subsequent parametric studies of the risk likelihood. Although a stationary wind field is assumed, the approach remains valid for wind gusts or urban canyon effects around obstacles in which case the wind velocity magnitude and direction should be different at different positions in the trajectory.

In future, Bayesian network will be implemented to identify the most frequent off-nominal conditions a UAV may be exposed to. Next, degraded controllability caused by the identified off-nominal conditions will be modeled and incorporated in the computation of the probability of obstacle collision instead of using an empirical value for control time. Besides, wind effect will be incorporated into the vehicle dynamic model in order to generate more precise values of trajectory deviation caused by wind. Effect of uncertainty in vehicle navigation measurements will be incorporated further in order to compute the risk of obstacle collision in real time. Finally, the risk formulation will be used to examine safe distance requirements for a UAV flight flying through urban canyons and variable wind conditions.

Acknowledgments

This work was supported by the System-Wide Safety (SWS) project under the Airspace Operations and Safety Program within the NASA Aeronautics Research Mission Directorate (ARMD). The authors thank Dr. Andrew Moore and Patrick Quach from the Dynamic Systems and Control Branch and the Safety Critical Avionics Branch at NASA Langley Research Center, for generating the UAV flight data.

REFERENCES

[1] I. Roychoudhury, L. Spirkovska, M. Daigle, E. Balaban, S. Sankararaman, C. Kulkarni, S. Poll, and K. Goebel, "Real-time monitoring and prediction of airspace safety," National Aeronautics and Space Administration, Tech. Rep., 2015.

[2] L. Spirkovska, I. Roychoudhury, M. Daigle, and K. Goebel, "Real time safety monitoring: Concept for supporting safe flight operations," in *17th AIAA Aviation Technology, Integration, and Operations Conference*, 2017, p. 4494.

[3] N. Aeronautics and S. Administration, "Nasa aeronautics strategic implementation plan: 2017 update." 2017.

[4] M. Corbetta, P. Banerjee, W. Okolo, G. Gorospe, and D. G. Luchinsky, "Real-time uav trajectory prediction for safety monitoring in low-altitude airspace," in *AIAA Aviation 2019 Forum*, 2019, p. 3514.

[5] P. Banerjee and M. Corbetta, "In-time uav flight-trajectory estimation and tracking using bayesian filters," in *2020 IEEE Aerospace Conference*. IEEE, 2020, pp. 1–9.

[6] M. Daigle and C. S. Kulkarni, "End-of-discharge and end-of-life prediction in lithium-ion batteries with electrochemistry-based aging models," in *AIAA Infotech@ Aerospace*, 2016, p. 2132.

[7] P. Banerjee, W. A. Okolo, and A. J. Moore, "In-flight detection of vibration anomalies in unmanned aerial vehicles," *Journal of Nondestructive Evaluation, Diagnostics and Prognostics of Engineering Systems*, pp. 1–8, 2020.

[8] E. Ancel, F. M. Capristan, J. V. Foster, and R. C. Condotta, "In-time non-participant casualty risk assessment to support onboard decision making for autonomous unmanned aircraft," in *AIAA Aviation 2019 Forum*, 2019, p. 3053.

[9] R. A. Clothier and R. A. Walker, "The safety risk management of unmanned aircraft systems," *Handbook of unmanned aerial vehicles*, pp. 2229–2275, 2015.

[10] R. Weibel and R. J. Hansman, "Safety considerations for operation of different classes of uavs in the nas," in *AIAA 4th Aviation Technology, Integration and Operations (ATIO) Forum*, 2004, p. 6244.

[11] A. Weinert, S. Campbell, A. Vela, D. Schuldt, and J. Kurucar, "Well-clear recommendation for small unmanned aircraft systems based on unmitigated collision risk," *Journal of Air Transportation*, vol. 26, no. 3, pp. 113–122, 2018.

[12] S. Primatesta, G. Guglieri, and A. Rizzo, "A risk-aware path planning strategy for uavs in urban environments," *Journal of Intelligent & Robotic Systems*, vol. 95, no. 2, pp. 629–643, 2019.

[13] B. Belkhouche, W. Al Ketbi, A. Al Neyadi, S. Al Nuaimi, and E. Al Hassani, "Modeling and virtualization of cultural heritage," in *2019 IEEE/ACS 16th International Conference on Computer Systems and Applications (AICCSA)*. IEEE, 2019, pp. 1–8.

[14] H.-T. Lee, L. A. Meyn, and S. Kim, "Probabilistic safety assessment of unmanned aerial system operations," *Journal of Guidance, Control, and Dynamics*, vol. 36, no. 2, pp. 610–617, 2013.

[15] J. Hu, "Probabilistic risk assessment and mitigation for uas safety and traffic management," in *Proceedings of the Annual Conference of the PHM Society*, vol. 11, 2019.

[16] E. Ancel, F. M. Capristan, J. V. Foster, and R. C. Condotta, "Real-time risk assessment framework for unmanned aircraft system (uas) traffic management (utm)," in *17th AIAA Aviation Technology, Integration, and Operations Conference*, 2017, p. 3273.

[17] F. A. Administration, "Safety management risk policy (faa order 8040.4b)," 2017.

[18] C. Valeriy and S. Ihor, "Method of the multi-uav formation flight control," *Archived Volume*, p. 167, 2018.

[19] S. D'Souza, A. Ishihara, B. Nikaido, and H. Hasseeb, "Feasibility of varying geo-fence around an unmanned aircraft operation based on vehicle performance and wind," in *2016 IEEE/AIAA 35th Digital Avionics Systems Conference (DASC)*. IEEE, 2016, pp. 1–10.

[20] V. Ilci and C. Toth, "High definition 3d map creation using gnss/imu/lidar sensor integration to support autonomous vehicle navigation," *Sensors*, vol. 20, no. 3, p. 899, 2020.

BIOGRAPHY

Portia Banerjee *received her Bachelors of Technology degree in Electronics and Communications Engineering from National Institute of Technology Durgapur, India and her Ph.D. in Electrical and Computer Engineering from Michigan State University. She is currently working on health monitoring of unmanned aviation systems as a research engineer with KBR. at NASA Ames Research Center, CA. Her research interests include statistical signal processing, image processing, data mining, uncertainty management and reliability analysis focusing towards diagnostic and prognostic applications in structures and autonomous systems. She is a member of the AIAA, IEEE and ASME societies and is a member of the Executive Committee of ASME NDE Diagnosis and Prognosis Division.*

George Gorospe *received his B.S. in Mechanical Engineering from the University of New Mexico in 2012. He has been a member of the Diagnostics and Prognostics Research Group at NASA Ames Research Center since 2012. His current research interests include, advanced automated testing, health-aware autonomy, and hardware accelerated computing.*

Ersin Ancel *received his B.S. from Istanbul Technical University and M.S. from Old Dominion University in Aerospace Engineering in 2005 and 2007, respectively. He received his Ph.D. from Old Dominion University in Engineering Management and Systems Engineering in 2011. His research interests include commercial aviation safety and accident modeling, airspace separation assurance functional allocation, and UAS/UAM risk assessment and mitigation.*